In situ visualization of ionic liquid electrospray emission using transmission electron microscopy

Kurt J. Terhune* and Lyon B. King†,
Michigan Technological University, Houghton, MI, 49931, USA

Kai He‡ and John Cumings§§
University of Maryland, College Park, MD, 20742, USA

***In-situ* observation of an operating ionic liquid electrospray emitter was achieved using a LaB_6 transmission electron microscope. The emitter was an electrochemically etched tungsten needle that was externally wetted with the ionic liquid OMIM-BF_4. During both positive and negative emission solid dendritic structures were created and left behind at the emission sites. These structures were seen to grow on timescales of a few minutes. It is possible that depletion of one ion species (cation or anion) from the emission region drastically changed the physical behavior of the propellant left behind, possibly resulting in solidification of a new chemical substance at the emission site. This solidification may be independent of any interaction with the metallic substrate. Such observations have not been witnessed in electrospray research, and though the underlying cause is presently unknown the molecular structure of the ionic liquid most likely plays a role. A final observation was that a majority of the emission sites during BF_4^- and $OMIM^+$ operation were at locations along the shaft of the tungsten needle instead of the cone apex.**

Nomenclature

d	=	extraction distance
E	=	electric field
I	=	electrical current
r	=	radius of Taylor cone apex
V	=	electric potential

I. Introduction

ELECTROSPRAY thrusters are attractive because of their high efficiency and potential for widely variable thrust-to-power ratio.[1,2] There are two families of electrospray propellants: liquid metals such as indium,[3] gallium,[4] gallium-indium,[5,6] and gold,[7] and ionic liquids, such as EMIM-BF_4,[1,2,8-12] EMIM-IM,[2,8,11,13,14] and BMIM-PF_6.[15,16] Ionic liquids are room-temperature molten salts with high electrical conductivity and almost zero vapor pressure, making them ideal for operating in a vacuum.[17] Furthermore, their numerous cation/anion combinations can provide a broad spectrum of operating parameters.[18-20]

Broadly speaking, there are two designs for ionic-liquid electrospray thrusters: internally-wetted and externally-wetted needles. Both designs have advantages and disadvantages. Internally-wetted designs use either actively-[1,9,13] or passively-driven[2] techniques to force the ionic liquid through a capillary and to the capillary orifice where it is extracted by either an AC[21] or DC electric field. Externally-wetted thruster designs have a microfabricated solid sharp feature, either in the form of a needle or cone, which provides the emission site for the electrospray. The propellant reaches the emission site by flowing over the external surface of the needle in a thin layer, hence the propellant liquid must be "wetting" on the solid.[22,23]

* PhD Pre-Candidate, Mechanical Engineering-Engineering Mechanics, 815 RL Smith Building, Student Member.
† Ron and Elaine Starr Professor in Space Systems in Engineering, Mechanical Engineering-Engineering Mechanics, 1014 RL Smith Building. AIAA member.
‡ Assistant Research Scientist, Department of Materials Science and Engineering, Bldg. 90, Stadium Dr.
§ Associate Professor, Department of Materials Science and Engineering, Bldg. 90, Stadium Dr.

A. Theoretical operation of electrosprays

The established theory of operation suggests that electrospray thrusters emit ions and/or charged droplets through the formation of conical liquid protrusions produced when a strong electric field pulls on the surface of the IL through electrostatic traction. These "remarkably stable conical features are called Taylor cones"[24], eponymous with G. I. Taylor who studied them extensively starting in the 1960's.[25] The formation comes from a balance of the electrostatic force and the local surface tension at the surface of the liquid. The Taylor cone itself is not a static feature, and thus depending on the conditions of its formation, operates in multiple modes and regimes.[26] In electrospray research, the most relevant mode is the cone-jet mode. In this mode, charge accumulates at the apex of the Taylor cone and is extracted by the electric field in the form of a thin jet, which then breaks into charged-droplets and ions.

While the bulk electric field between the Taylor cone and the electrode can be estimated during an experiment based on geometry and applied voltage, the critical parameter for electrospray is the local electric field that exists at the tip of the cone-jet apex of the structure. The field at the tip will differ by orders of magnitude from the bulk field because the sharp liquid tip acts to amplify the field near the cone apex. The field has typically been estimated based on models that make assumptions about the liquid cone-jet geometry.[27,28] The challenge with deriving a suitable model comes from the fact that the ionic liquid surface behaves like a deformable electrode, where the local electric field and the radius of the cone tip are both dependent on the other, as seen in Figure 1.

.

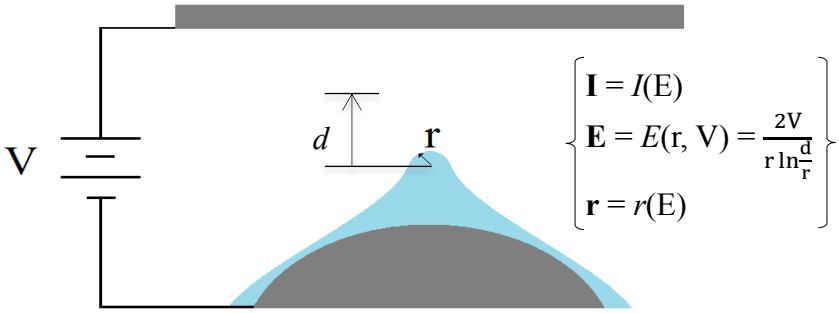

Figure 1. The formation of a Taylor cone depends on the geometric enhancement of the local electric field. The enhanced field depends on the radius of the tip, r, which, in turn, is a function of the electric field.

As Figure 1 illustrates, the formation of a Taylor cone, specifically the region including the cone apex, is the critical element in the operation of electrosprays. This cone-jet formation occurs on the sub-micron scale, which makes it difficult to directly observe the spray emission process.

Another challenge in electrospray operation is the electrochemical fouling of electrode surface. Such surface degradation has been reported by several groups while operating ionic liquid electrosprays.[21,29-31] The current theory is that during prolonged single polarity emission a double layer forms in the liquid near the electrode surface. Once the charge of the interfacial double layer exceeds the electrochemical window of the IL, electrochemical degradation of the surface occurs. The current mitigation technique is to operate the thruster in alternating polarity at 1 Hz.

B. In-situ Visualization of Electrosprays

In-situ visualization of electrosprays has been achieved using several instruments and imaging techniques. The use of optical microscope and video cameras has provided visual results that are used for modeling and characterization of these devices.[7,32] However, the behavior of the liquid within a few microns of the cone apex cannot be observed using optical techniques and thus the most important spray physics are inaccessible to optical diagnostics. Electron microscopy is necessary to observe the features and dynamics at the emission site. While it is challenging to operate an electrospray source within an electron microscope, several groups overcame this challenge, and have been able to produce Taylor cone/jet emission in the specimen chamber of a TEM using liquid metal ion sources (LMIS). This allowed these groups to capture *in-situ* visualizations of an operating Taylor cone using gold,[33] lead,[34] tin,[35] gallium,[36] indium,[37] gold-germanium alloy,[38] and cobalt-germanium alloy[39] ion sources. Such direct observation enabled researchers to verify the fundamental structure of the cone/jet emitter; specifically, cone-angle, jet length, and jet angle were measured at varying levels of emission current of the ion source. These observations agreed with the theoretical operation of electrosprays.

C. Ionic Liquid Electrosprays

The underlying physics of ionic liquid electrosprays is generally assumed to be the same as that of liquid metal electrosprays. In particular, the spray is usually described by standard fluid models and cone/jet formation is dependent upon the fluid electrical conductivity, surface tension, and viscosity since these fluid models have been successfully used to characterize liquid metal sprays.[1,2,29,40] However, ionic liquids are fundamentally different from liquid metals in that they are comprised of large molecules as opposed to single atoms.[17,41] The interactions between these molecules can be very complicated; this is especially important since the emission apex of an electrospray cone/jet has features on the order of the molecular size. Understanding how molecular structure pertains to the operation of electrospray and the critical cone apex region of a Taylor cone has been an unexplored facet of ionic liquid electrospray research. The goal of research reported here was to directly observe the fluid features in the emission region of an ionic liquid electrospray source with image resolution on the order of the molecular size.

II. Experimental Methods and Apparatus

An experiment using an electrospray apparatus consisting of a solid tungsten needle wetted by a thin external layer of ionic liquid was performed within a TEM to accomplish this goal. The specifics of the microscope facilities and the electrospray apparatus are described in the sections II-A and II-B. The procedure for the experiment is provided in section II-C.

A. Facilities

The University of Maryland's Nanoscale Image Spectroscopy and Properties Laboratory (NISP Lab) houses the TEM that was used in this research. The JEOL JEM-2100 LaB_6 TEM is a multi-purpose transmission electron microscope that has a LaB_6 thermionic emission electron source, which provides a relatively high beam current for the given probe size. The electron beam can be accelerated to 80, 100, 120, 160, or 200 keV. The beam energy chosen for this experiment was 200 keV. The images produced by the microscope can be captured via film or a CCD camera, and the instrument has a point-to-point resolution of 0.23 nm.[42] The specimen chamber is kept at a pressure of 10^{-6} Torr.[43]

B. Electrospray Apparatus for TEM

An electrospray emitter was designed to be compatible with a Nanofactory *in-situ* STM-TEM™ holder. To accomplish this, a tungsten needle with a tip radius of approximately 1-μm was fabricated through an electrochemical etching process using a 3M NaOH solution. An etched needle similar to the device used for the TEM studies is shown in Figure 2.a) to illustrate the surface features produced by the etching process. The etched needle was potted in a brass TEM sample-holder stub using silver epoxy. The brass stub-needle assembly was held in place by interference fit in a brass tube fixed to the biased side of the sample holder. The junction of the tungsten needle and the face of the brass stub formed an inside corner geometry that acted as a capillary reservoir to hold a small drop of the IL, Figure 2.b) The IL chosen for this experiment was 3-methyl-1-octylimidazolium tetrafluoroborate (OMIM-BF_4).

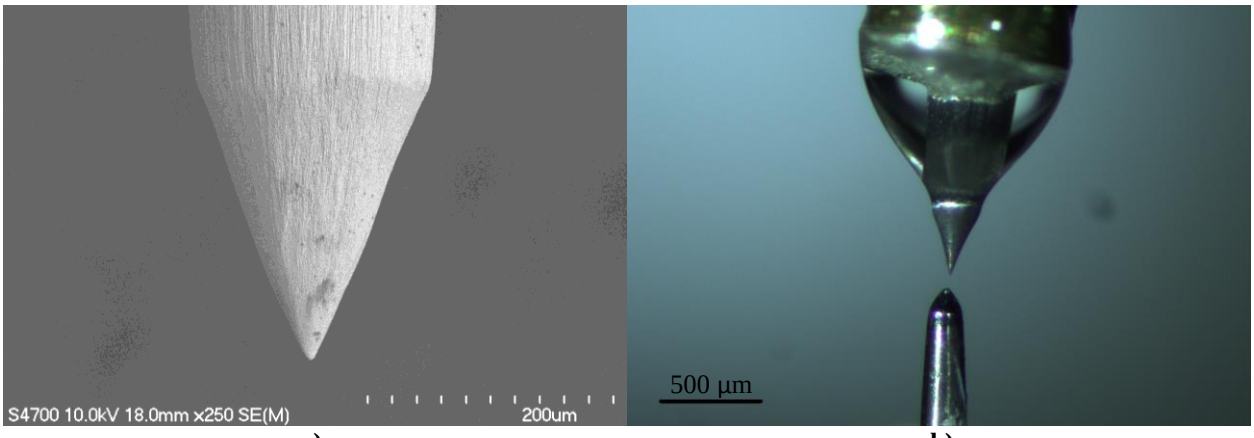

a) **b)**

Figure 2. a) An SEM micrograph of a tungsten needle produced using a 3M NaOH etching process. Note the striations etched in the axial direction of the needle. b) An optical image of the tungsten needle potted in the brass stub illustrating the capillary reservoir for IL created by the junction of the two materials.

The counter-electrode was a platinum wire turned down to a cone with a sub-100-μm tip radius, inserted through an aluminum sheet such that it extended about 250 μm from the surface. The platinum wire was held in place using silver epoxy. The aluminum sheet was then bent into a U-shape to provide a large fixed-potential plane in the vicinity of the needle tip. The electrode was manipulated in three dimensions by pulsing a piezoelectric rod. The setup is shown in Figure 3. Either the tungsten needle or the counter-electrode can be biased using a Keithley 2410 power supply with a range of -1.1 kV to +1.1 kV.

Figure 3. The electrospray setup with tungsten needle coated with OMIM-BF_4 (image-left), the U-shaped aluminum sheet-platinum wire counter-electrode (image center) and the holder hat (image-right).

C. Experimental Procedures

After etching, the tungsten needle was cleaned in a sonic bath of acetone followed by a sonic bath of isopropyl alcohol to remove any foreign materials. The needle was then dipped into a droplet of OMIM-BF_4 and inserted into the TEM holder. The piezo-hat, with the counter-electrode already inserted, was then placed on the ball of the piezo-driven arm, and manipulated into a position such that any movement while in the TEM was within the limits of the piezoelectric motor.

The holder was then inserted into the TEM and leads for the piezo drive and power supply were attached. The counter-electrode was positioned such that it was in the same plane as the tungsten needle, and at a distance of 10 μm away from the apex of the needle, as shown in Figure 4.

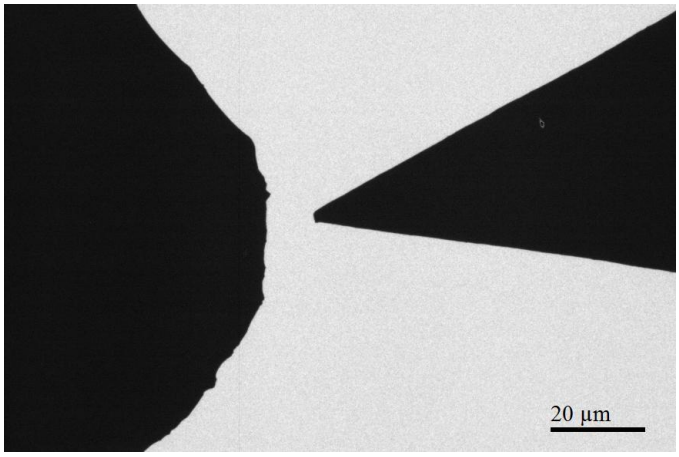

Figure 4. A TEM image of emitter needle (image-right) positioned at a distance of 10 μm from the counter-electrode (image-left).

Once the position of the counter-electrode was fixed the bias of the needle was increased in 50 V steps to a positive 1000 V, or until emission current was observed. When emission current was observed, the sample was shifted in the plane normal to the beam until the operating emission site of the electrospray was located. Images were then taken when the needle was biased at various potentials while recording video and telemetry. Following this, the needle bias was reduced to 0 V at 50 V intervals. The process was then repeated—without breaking vacuum—for a negative bias of maximum -1000 V.

III. Results

The results from the positive-polarity emission and the negative-polarity emission TEM tests will be presented in sections III-A and III-B, respectively.

A. *In-situ* Observation of Positive-Polarity Emission

The applied voltage and collected electrospray current were recorded for the duration of the test and are included in Figure 5. Current emission was first observed at 925 V during the initial ramp up to 1000 V. The emission was initially intermittent which motivated an increase to 1000 V. Stable emission current was not immediate. Prolonged biasing of the needle for upwards of 5 minutes was required prior to the stabilization of emission current. A steady increase in emission current without an increase in applied voltage was also observed during several intervals throughout the test.

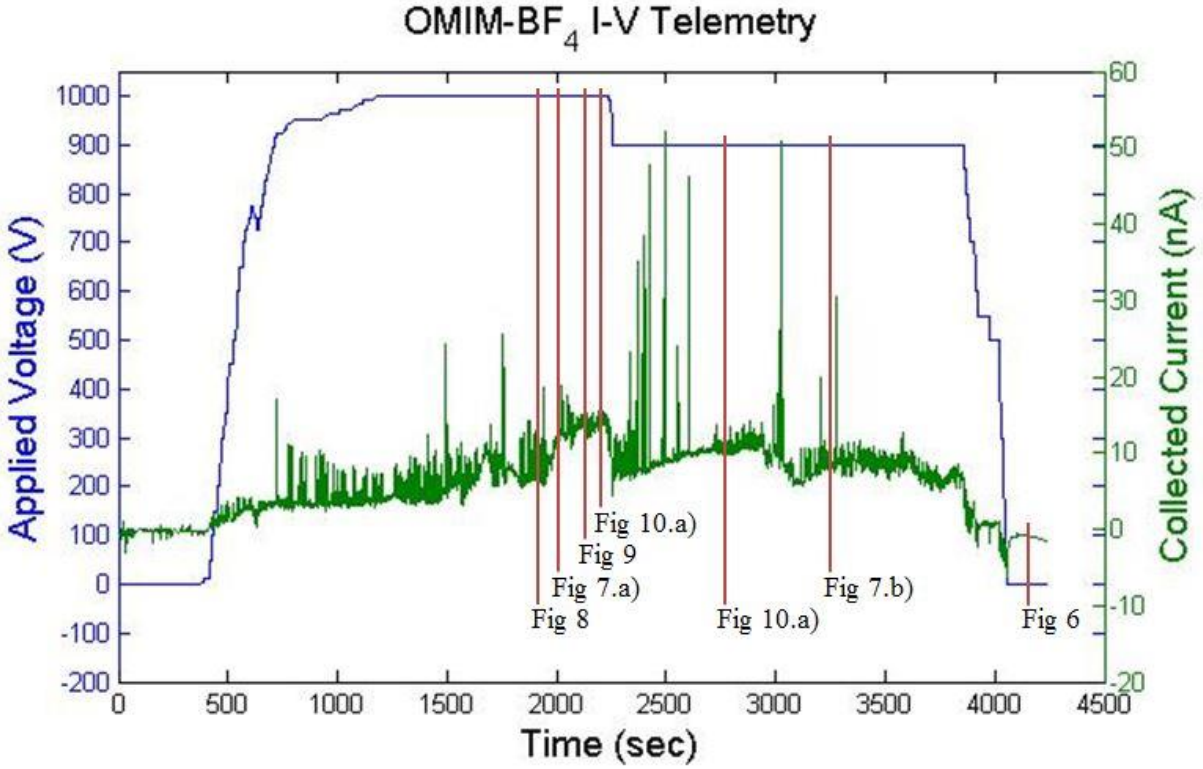

Figure 5. Applied voltage and collected current for the positive-polarity emission test. Markers show collection times for subsequent images.

During the stable emission, growths along the surface of the tungsten needle were observed. Surprisingly, a majority of these growths occurred at various locations along the needle cone surface instead of solely at the needle apex. Therefore, an illustration noting the locations of the features presented in this section is provided in Figure 6. It should be noted that Figure 6 was recorded at the end of the test sequence shown in Figure 5 and that the features shown are likely solidified in this image (see discussion in Section IV-A) – however this low-magnification image provides context and geometric orientation for discussion of Figure 7 - Figure 10.

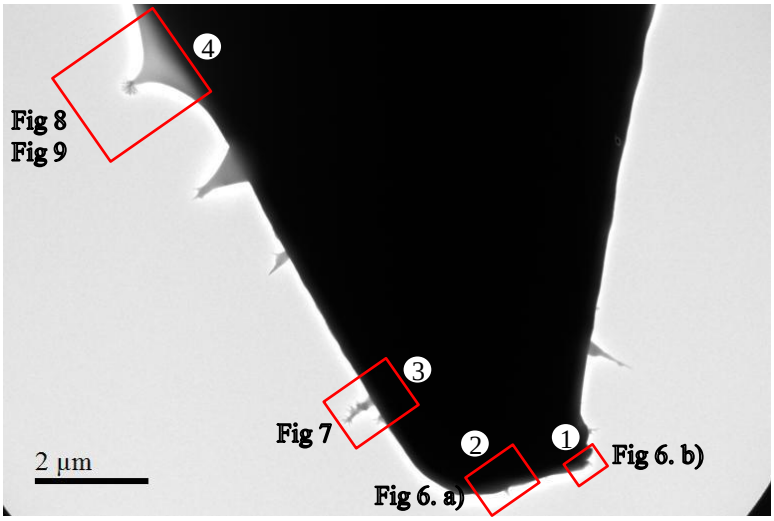

Figure 6. A TEM image of the tungsten needle after positive-polarity emission. Regions of interest and the corresponding figures presented in the following section are denoted in the image.

The feature in region 1 was one of the only features observed in the apex region of the needle. This region is shown in Figure 7, where it is evident that the geometry is not a classical Taylor cone/jet, but instead resembles a dendritic solid structure.

Another feature in region 3 extended in a direction normal to the surface; the detail of this region is shown in Figure 8. This feature has similar dendritic structures seen in the feature in region 1, however, the length is an order of magnitude larger.

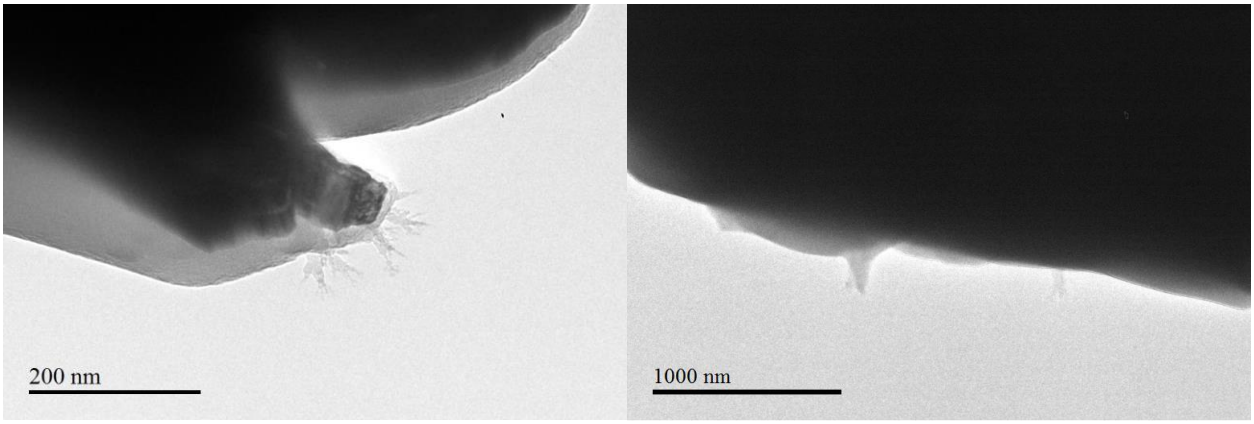

a) **b)**

Figure 7. TEM images of dendritic growth in a) region 1 and b) region 2 in the apex region of the tungsten needle. The tungsten needle potential was 1000 V.

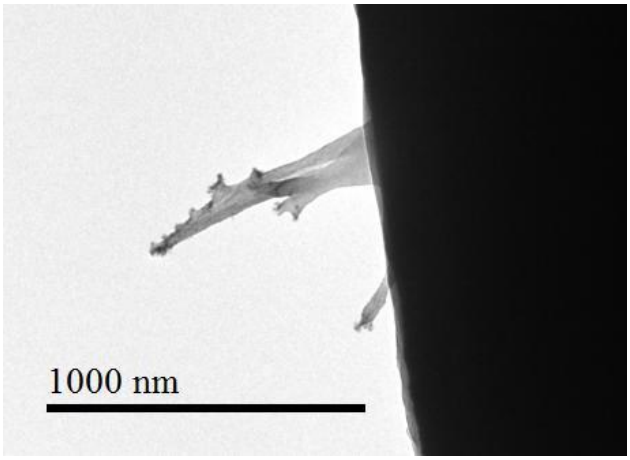

Figure 8. A TEM image of a dendritic growth in region 3 on the tungsten needle. The location is approximately 2 μm from the apex region.

A relatively large feature was observed in region 4 on the tungsten needle and was imaged in higher magnification in Figure 9. The position is approximately 8 μm from the apex region. In the initial observation the feature appeared be a Taylor cone[**] conical feature. However, as time progressed the apex of the cone began to form the dendritic features seen at the other locations; this is shown in Figure 10.a). This growth pattern continued for 25 minutes until the rate of growth slowed, Figure 10.b).

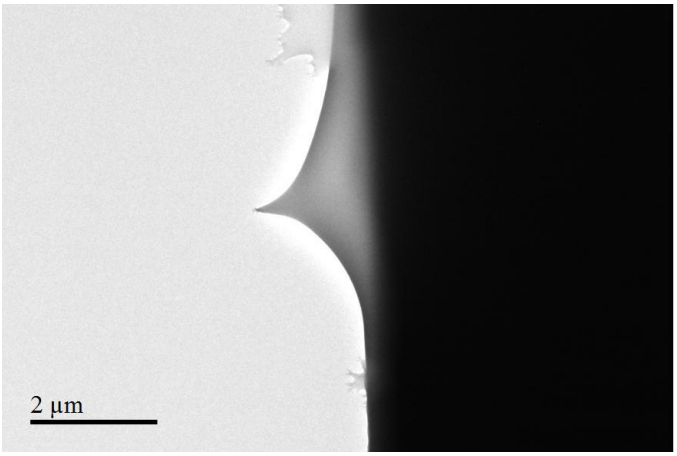

Figure 9. A TEM image of a Taylor cone at location (4) on the tungsten needle. The tungsten needle potential was 1000 V.

A final observation can be made on appearance of the tungsten needle after the potential was returned to 0 V. Although Figure 6 was presented first in this discussion, the image was actually recorded after emission testing was completed and there is no electric field and, hence, no emission current occurring during the image. This strongly suggests that the features that were observed during emission remained on the surface and formed some type of solid or at least visco-elastic gel. Each individual spray emission site left a solid structure behind on the surface of the needle.

[**] For convenience, the term 'Taylor cone' will be used henceforth to describe similar conical features seen in the images even though the features don't strictly adhere to Taylor cone geometry.

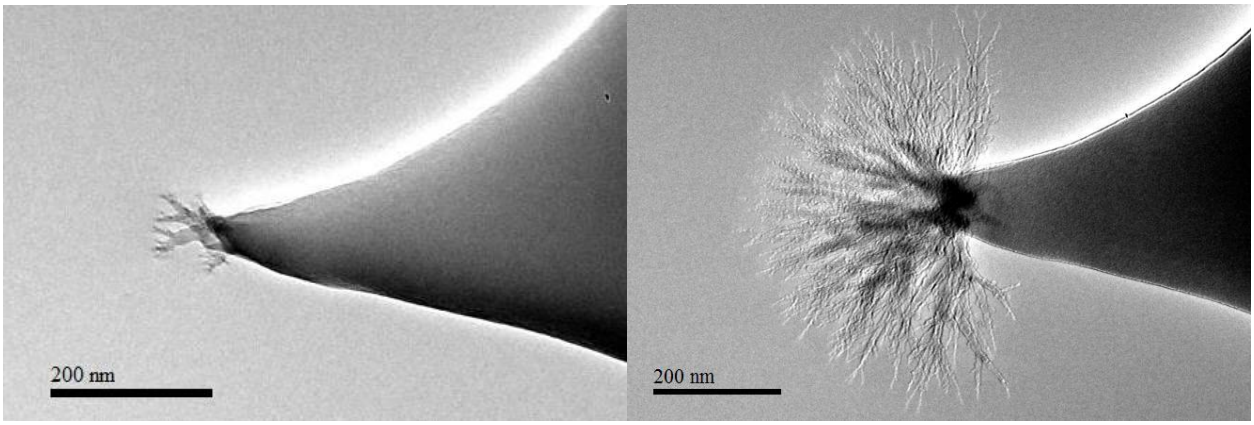

a) **b)**

Figure 10. TEM images of the conical feature at region 4 on the needle showing the dendrite growth over an elapsed-time of 10 minutes from a) to b). The tungsten needle potential was 1000 V for 3.5 minutes and then was decreased to 900 V for remainder of the elapsed-time.

B. *In situ* Observation of Negative-Polarity Emission

The negative-polarity emission tests were performed directly subsequent to the positive polarity emission without change of needle. This means that the solid structures left behind by the positive test certainly influenced emission during the negative tests. The applied voltage and collected electrospray current were recorded for the duration of the negative-polarity emission test and are included in Figure 11. Current was first observed at -1000 V but was intermittent. Similar to the positive-polarity emission test, the needle needed to be biased for a prolonged period before stable emission was recorded. A steady increase in emission current without an increase in applied voltage was also observed.

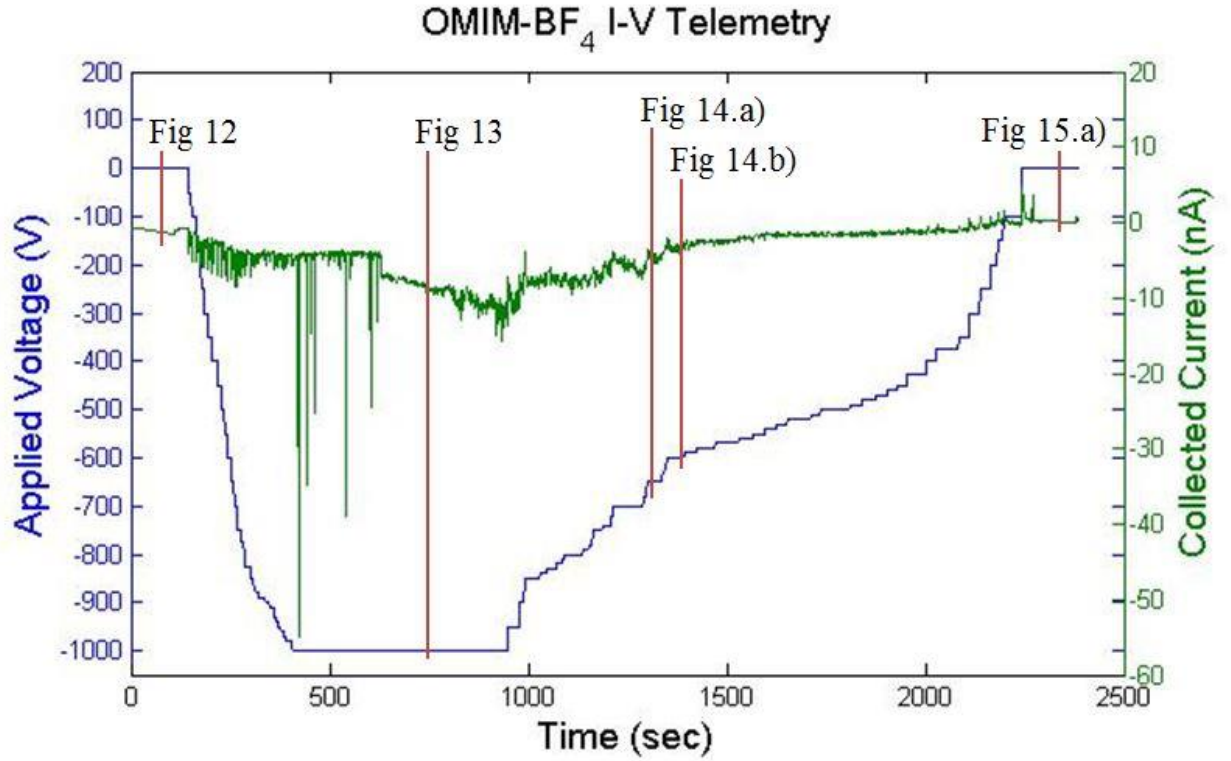

Figure 11. Applied voltage and collected current telemetries for then negative-polarity emission test. Markers show collection times for subsequent images.

During the stable emission, growths along the surface of the tungsten needle were observed. Similar to the positive-polarity test, a majority of these growths occurred at various locations along the needle shaft instead of solely at the needle apex. Therefore, Figure 12 is provided to illustrate the regions-of-interest and the locations of electrospray emission, along with the corresponding regions of the figures given in the remainder of the section. The image used in Figure 12 was captured prior to the start of the negative polarity test.

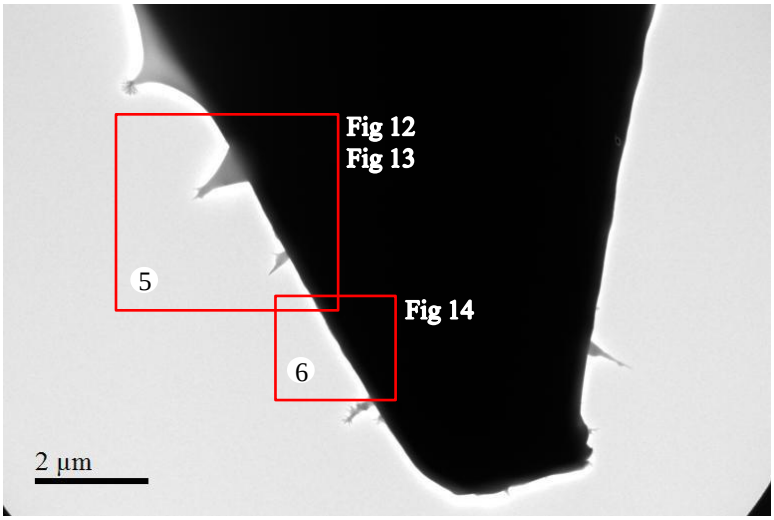

Figure 12. A TEM image of the tungsten needle prior to the start of the negative-polarity emission test. The regions of interest and corresponding figures presented in the following sections are denoted in the image.

The remnant features from the positive-polarity test appeared to provide a location for the IL to propagate, and thus one of the two emission sites imaged was originally the feature at region 3 in Figure 6, and also within region 5 of Figure 12. The IL propagated up the original feature and then expanded outward, as illustrated in Figure 13.

The location that the IL propagated became an emission site, and what appeared to be Taylor cones forming, emitting and relaxing. However, this cycle ceased after several minutes of emission and the conical features solidified on the surface, seen in Figure 14.a).

In region 6, IL that propagated on the smooth surface of the needle began to produce Taylor cones operating in an apparent breathing mode, seen in Figure 14.a); the needle potential was -650 V. When the needle potential was reduced to -600 V, a large Taylor cone formed and appeared to be operating stably, but as time progressed the feature became static, shown in Figure 14.b).

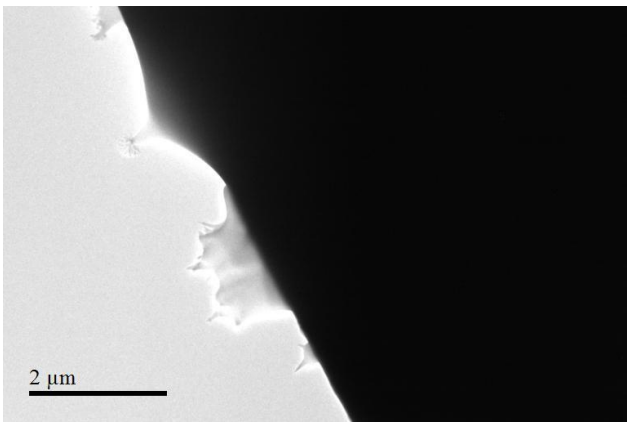

Figure 13. TEM images of feature growth during negative-polarity emission testing. An elapsed-time of 8 minutes at an applied potential of -1000 V produced the growth on the feature originally seen in region 5 of Figure 12.

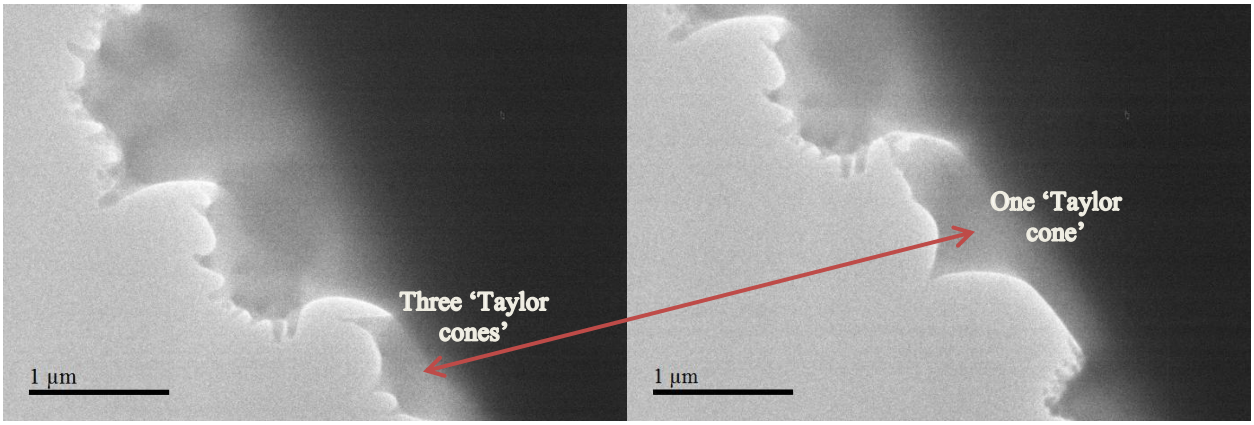

a) **b)**

Figure 14. TEM images of a) the multiple solidified cone-features and multiple operating Taylor cones, and b) a single operating Taylor cone. The needle potential was a) -650 V and b) -600 V.

A final observation for this test can be made regarding the appearance of the tungsten needle after the test was complete. At low magnification it can be seen that several remnants from emission remain on the surface, Figure 15.a). A post-test image of the tungsten needle captured using an SEM also shows these remnants, Figure 15.b). This is further evidence that solidification of IL or some chemical substance created by the interface of the IL with tungsten occurs during emission.

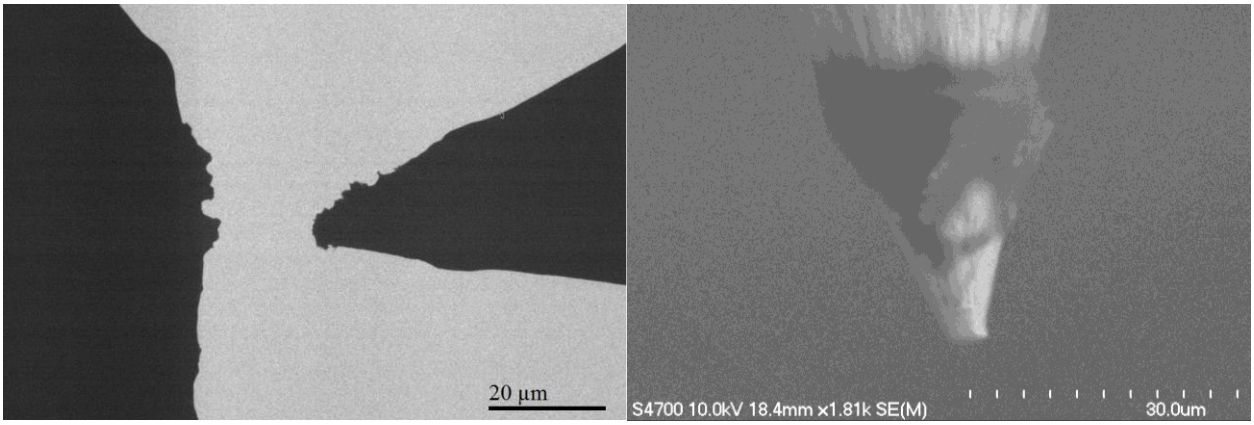

a) **b)**

Figure 15. a) A TEM image of the tungsten needle and counter-electrode after the completion of positive-polarity and negative-polarity emission tests. b) An SEM micrograph of the needle after the completion of the emission tests.

IV. Discussion

The results from the emission testing in the TEM have produced several observations concerning the operation of an externally-wetted ionic-liquid electrospray thruster. As the *in-situ* visualization of an ionic-liquid electrospray thruster in a TEM has never been achieved in prior research, any of the observations presented in this paper are novel. These findings will be discussed in the following sections.

A. Accumulation of Emission Byproducts

The solidification of the IL during the emission testing was not something predicted in prior research. Previously, it was thought that the ionic liquid retracted from emission sites or formed isolated droplets on the emitter surface after the extraction potential was removed.[29] This experiment, however, shows that the ionic liquid and/or its interaction with the tungsten needle form solid features during emission which remain upon removal of an applied potential.

The overall accumulation of emission byproducts (dendritic or conical features) on the surface of the tungsten needle can be seen by comparing the images in Figure 4, Figure 6, and Figure 16. The extent of byproduct

accumulation is more predominant in the negative-polarity testing, but this could be an effect of the order of emission testing (positive-polarity followed by negative-polarity). The surface features produced by the positive-polarity test could have provided a better wetting surface for the IL in the negative-polarity test.

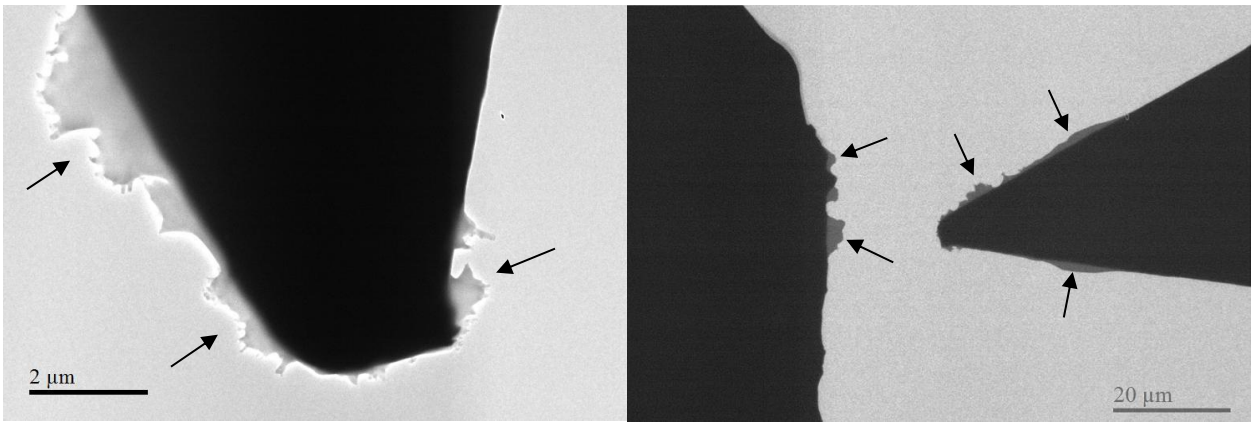

a) **b)**

Figure 16. TEM images visualizing the accumulation of emission byproducts on the surface of the tungsten needle and the end of electrospray emission tests. a) The appearance of tungsten needle after both positive-polarity and negative-polarity emission tests, and b) the final TEM image of the tungsten needle after emission tests overlaid on the initial TEM image to show the accumulation on the surface. The light-gray areas indicated by arrows represent the accumulation of emission byproducts.

During positive-polarity emission the solid features were in the form of dendritic branching structures. The cause of this is presently unknown, though one theory is that ionic liquids exist with mesoscopic structures which could affect the dynamic process of extracting ion clusters from the emitter.[41] Studies[44,45] on the polarity of imidazolium-based ionic liquids have shown that the cation has relatively high polarity, which could be another factor in the growth of the dendritic structures. For negative-polarity emission, there is an absence of dendritic structures, suggesting a different cause than mesoscopic structures. One possibility is the drastic size difference between the OMIM cation and the BF_4 anion. The OMIM cation has a relatively long butyl chain extending from an imidazolium ring as opposed to the BF_4 anion which consists of one boron atom bonded to four fluorine atoms; this could lead to BF_4 having higher mobility.

Whatever the cause, changes in the surface cannot be ignored and will eventually affect the operation of the electrospray thruster. This conclusion has been made previously,[21,30] but the extent of this visualization provides further evidence of this and direct observation of the growth process.

B. Dendritic Growth

As mentioned in section III-A, dendritic growth was only seen during positive-polarity emission. The rate of the dendritic growth during emission was such that it could be seen in real-time. The growths appear to form at any of the emission sites, and continue to branch until the electric field is removed. The growth is illustrated in Figure 17.

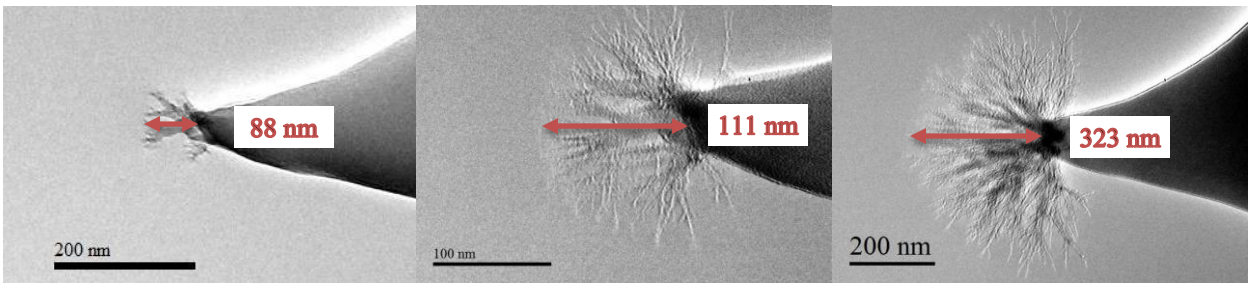

Figure 17. TEM images illustrating the dendritic growth during positive polarity. The time-lapsed since the start of the test is a) 18, b) 21, and c) 27 minutes. The needle bias is a) 1000 V, b) 900 V, and c) 900 V.

C. Taylor Cone Formation and Solidification

The formation of Taylor cones during negative-polarity emission testing adheres to the theoretical operation of externally-wetted IL thrusters. As noted in previous research[26], higher extraction potentials produce multiple Taylor cones operating unstably. This was seen in the negative-emission test and the correlation is illustrated by Figure 13 and Figure 14. Taylor cones would form and appear to emit in the form of a jet, and then relax back into the liquid reservoir on the surface of the tungsten needle; this formation/relaxation repeated at rate of approximately once every 2 or 3 seconds. This was most likely due to high extraction potentials which pulled the liquid from the surface at a rate too quickly for capillary flow to replenish the liquid to the emission site, Figure 18.a).

Also noted in past research was that lower potentials reduced the instability of Taylor cones, eventually leading to Taylor cones that appeared to operate in the cone-jet mode. A stable Taylor cone at region 6 formed at a lower potential of -650 V. The size of the Taylor cone was much larger than those at region 5 because it was emitting from liquid on the surface of the tungsten needle, instead of the surface of a dendrite, which provided a large radius of curvature. The operating Taylor cone is seen in Figure 19.a).

A completely new finding in this research is the observation that the emission cone/jet features remained permanent after the electric field was removed. In both modes of operation, the Taylor cones are seen to solidify. This is illustrated in Figure 18.b) and Figure 19.b). This observation is evidence that the molecular structure of ionic liquids plays an important role in electrospray emission.

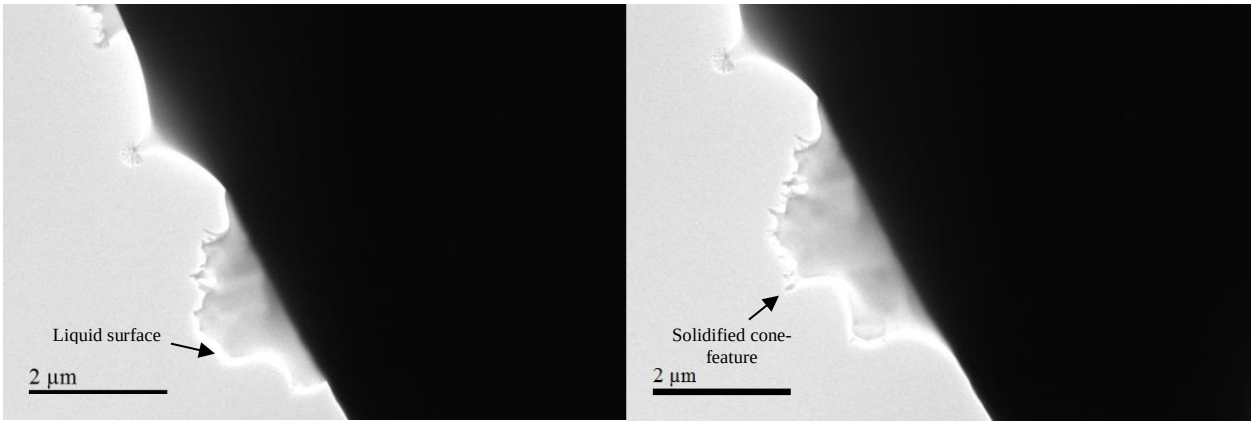

a) b)

Figure 18. TEM images taken at region 5 showing a) surface of the liquid where Taylor cones formed and relaxed, and b) solidified cone-features on the surface.

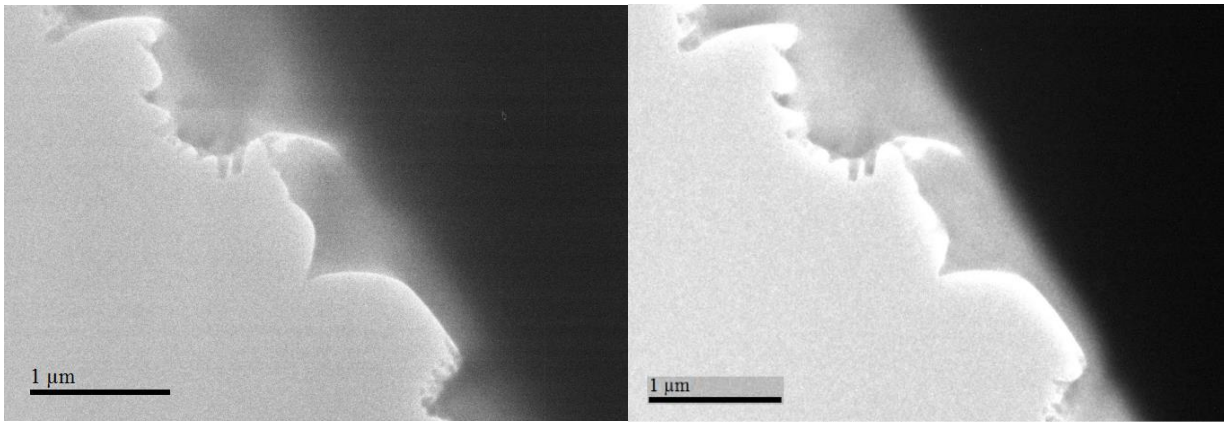

a) **b)**

Figure 19. TEM images of stable Taylor cone a) operating at -650 V, and b) static at 0 V, evidence that solidification occurred.

V. Conclusion

An electrospray apparatus was fabricated for use in a transmission electron microscope and *in-situ* observation of positive-polarity and negative-polarity ionic-liquid electrospray emission testing was achieved. The ionic liquid used in the emission tests was OMIM-BF_4, which allowed for lower extraction potentials than ionic liquids typically used in electrospray studies. The *in-situ* observations acquired were the first visualization of an ionic liquid electrospray within nanometers of the emission site. The formation of dendritic solid structures was observed during the positive-polarity emission test and the formation of Taylor-cone-like features was observed during the negative-polarity emission test. During each test the ionic liquid or separate byproducts from emission appeared to solidify on the surface of the needle. This has not previously been observed in LMIS electrosprays, suggesting that the spray physics of ILs is much different than that of liquid metals. These observations are evidence that ionic liquids cannot be treated as simple fluids, but instead the molecular structure must be considered in the process of electrospray.

The accumulation of emission byproducts, while mentioned in prior studies, had never been examined on this scale. While it has long been accepted that the interface between the ionic liquid and the metal substrate can be modified by electrochemical reactions it was believed that this modification manifested as a surface layer; in this work it was shown that the electrochemistry occurs at the apex of the emitter in the liquid phase. It is likely that depletion of one ion species (cation or anion) from the emission region drastically changes the physical behavior of the propellant left behind, possibly resulting in solidification of a new compound at the emission site. This solidification may be independent of any interaction with the metallic substrate. The formation of dendritic features has not been previously mentioned in theoretical operation of electrospray thrusters and could change the understanding of how ionic liquid electrosprays operate. Future studies should include a more thorough examination of electrospray emission in TEM, including a similar experiment where negative-polarity emission testing precedes positive-polarity emission testing and also tests in which the polarity is switched on a timescale short compared to the electrochemical window—for instance 1 Hz. It would also be instructive to compare the solid features produced by different ionic liquids and different metallic substrates. Lastly, the molecular structure of ILs, specifically imidazolium-based ILs should be conducted to determine any affects it may have on electrospray operation.

Acknowledgments

Authors K.T. and L.K. would like to thank members of the Michigan Tech's ISP Lab for all the thought-provoking discussions, specifically Robert Washeleski for his helpful advice on image processing, Edmond Meyer and Brandon Jackson for their guidance in MATLAB programming, and Mark Hopkins for his help with LabView data acquisition and programming. They would also like to thank Dr. Reza Shahbazian Yassar and Qi Gao for their extensive help with the TEM in Michigan Tech's ACMAL facility. A special thanks to Dr. Jason Makela for all of his guidance on electrospray devices and electron microscopy, Owen Mills for electron microscopy advice, Marty Toth for machining all custom components for the experiments, and the members of University of Maryland's NispLab, including, Khim Karki for his help while using the TEM and Dr. Wen-An Chiou for permitting the experiments to be performed in their TEM. Lastly, they would like to acknowledge the support from the Michigan/Air Force Center of Excellence in Electric Propulsion for this research.

Authors K.H. and J.C. acknowledge support by the Science of Nanostructures for Electrical Energy Storage, an Energy Frontier Research Center funded by the US Department of Energy, Office of Science, Office of Basic Energy Sciences under Award Number DESC0001160. They also acknowledge the use of facilities in Maryland NanoCenter and its NispLab, supported in part by the NSF MRSEC under grant DMR 05-20471.

References

1. Lozano, P.C., "Studies on the Ion-Droplet Mixed Regime in Colloid Thrusters," Department of Aeronautics and Astronautics, Massachusetts Institute of Technology, 2003
2. Legge, R.S., Jr., "Fabrication and Characterization of Porous Metal Emitters for Electrospray Applications," Department of Aeronautics and Astronautics, Massachusetts Institute of Technology, 2008
3. Makela, J.M., "Re-generable Field Emission Cathodes for Electric Propulsion," Mechanical Engineering – Engineering Mechanics, Michigan Technological University, 2010
4. Forbest, R.G., "Understanding how the liquid-metal ion source works," Vacuum, 48, 1997, pp. 85-97
5. Thompson, S.P. and P.D. Prewett, "The dynamics of liquid metal ion sources," Journal of Physics D: Applied Physics, 17, 1984, pp. 2305
6. Ishitani, T., K. Umemura, and H. Tamura, "Mass and Energy Analyses of Gallium-Indium Liquid-Metal-Ion Sources," Japanese Journal of Applied Physics, 24, 1985, pp. L457-L454
7. Wang, K. and J.P.W. Stark, "Voltage effects on the nanoelectrospray characteristics in fully voltage-controlled atomisation of gold nanocolloids," Analytica Chimica Acta, 679, 2010, pp. 81-84
8. Krpoun, R. and H. Shea, "Microfabricated out-of-plane arrays of integrated capillary nano-electrospray emitters," *Transducers 2009*, Denver, CO, USA, June 20-24 2009
9. Chiu, Y.-H., et al., "Mass Spectrometric Analysis of Colloid Thruster Ion Emission from Selected Propellants," Journal of Propulsion and Power, 21, 2005, pp. 416-423
10. Garoz, D., et al., "Taylor cones of ionic liquids from capillary tubes as sources of pure ions: The role of surface tension and electrical conductivity," Journal of Applied Physics, 102, 2007, pp. 064913-10
11. Gassend, B., et al., "A Microfabricated Planar Electrospray Array Ionic Liquid Ion Source With Integrated Extractor," Microelectromechanical Systems, Journal of, 18, 2009, pp. 679-694
12. Terhune, K.J., Lyon B. King, "Ion and Droplet Mass Measurements of an Electrospray Emitter using an ExB Filter," *32nd International Electric Propulsion Conference*, Wiesbaden, Germany, 11 - 15 September
13. Chiu, Y.H., et al., "Vacuum electrospray ionization study of the ionic liquid, [Emim][Im]," International Journal of Mass Spectrometry, 265, 2007, pp. 146-158
14. Gamero-Castaño, M. and V. Hruby, "Electrospray as a Source of Nanoparticles for Efficient Colloid Thrusters," Journal of Propulsion and Power, 17, 2001, pp. 977-987
15. Dyson, P.J., et al., "Direct probe electrospray (and nanospray) ionization mass spectrometry of neat ionic liquids," Chemical Communications, 0, 2004, pp. 2204-2205
16. Jackson, G.P. and D.C. Duckworth, "Electrospray mass spectrometry of undiluted ionic liquids," Chemical Communications, 0, 2004, pp. 522-523
17. Baker, G.A., et al., "An analytical view of ionic liquids," Analyst, 130, 2005, pp. 800-808
18. Ghatee, M.H. and A.R. Zolghadr, "Surface tension measurements of imidazolium-based ionic liquids at liquid–vapor equilibrium," Fluid Phase Equilibria, 263, 2008, pp. 168-175
19. MacFarlane, D.R., et al., "Ionic liquids based on imidazolium, ammonium and pyrrolidinium salts of the dicyanamide anion," Green Chemistry, 4, 2002, pp. 444-448
20. Bini R Fau - Bortolini, O., et al., "Development of cation/anion "interaction" scales for ionic liquids through ESI-MS measurements," Journal of Physical Chemistry B, 2007, pp.
21. Lozano, P. and M. Martínez-Sánchez, "Ionic liquid ion sources: suppression of electrochemical reactions using voltage alternation," Journal of Colloid and Interface Science, 280, 2004, pp. 149-154
22. Garza, T.C., "Optimizing Wettability of Externally Wetted Microfabricated Silicon Electrospray Thrusters," Department of Aeronautics and Astronautics, Massachusetts Institute of Technology, 2007
23. Coffman, C.S., "Considerations for a multi-modal electrospray propulsion system," Department of Aeronautics and Astronautics., Massachusetts Institute of Technology, 2012
24. Fernández de la Mora, J., "The Fluid Dynamics of Taylor Cones," Annual Review of Fluid Mechanics, 39, 2006, pp. 217-243
25. Taylor, G.I., "The stability of a horizontal fluid interface in a vertical electric field," Journal of Fluid Mechanics, 2, 1965, pp. 1-15
26. Parvin, L., et al., "Electrospray Diagnostics by Fourier Analysis of Current Oscillations and Fast Imaging," Analytical Chemistry, 77, 2005, pp. 3908-3915
27. Gamero-Castaño, M. and J.F. de la Mora, "Direct measurement of ion evaporation kinetics from electrified liquid surfaces," The Journal of Chemical Physics, 113, 2000, pp. 815-832

28. Romero-Sanz, I., et al., "Source of heavy molecular ions based on Taylor cones of ionic liquids operating in the pure ion evaporation regime," Journal of Applied Physics, 94, 2003, pp. 3599-3605
29. Lozano, P. and M. Martínez-Sánchez, "On the dynamic response of externally wetted ionic liquid ion sources," Journal of Physics D: Applied Physics, 38, 2005, pp. 2371
30. Gassend, B.L.P., "A Fully Microfabricated Two-Dimensional Electrospray Array with Applications to Space Propulsion," Department of Electrical Engineering and Computer Science, Massachusetts Institute of Technology, 2007
31. Courtney, D.G., "Ionic Liquid Ion Source Emitter Arrays Fabricated on Bulk Porous Substrated for Spacecraft Propulsion," Department of Aeronautics and Astronautics, Massachusetts Institute of Technology, 2011
32. Alexander, M.S., et al., "Electrospray Performance of Microfabricated Colloid Thruster Arrays," Journal of Propulsion and Power, 22, 2006, pp. 620-627
33. Gaubi, H., et al., "Some new results about in-situ TEM observations of the Emission region in LMIS," *29th International Field Emission Symposium*, Stockholm, Sweden,
34. Driesel, W., C. Dietzsch, and M. Moser, "In-situ HV TEM observation of the tip shape of lead liquid metal ion sources," J. Phys. D: Appl. Phys, 29, 1996, pp. 2492-2500
35. Driesel, W. and C. Dietzsch, "In situ HVTEM observation of the tip shape of tin liquid metal ion sources," Applied Surface Science, 93, 1996, pp. 179-190
36. Driesel, W., et al., "HV TEM in situ investigations of the tip shape of a gallium liquid-metal ion/electron emitter," Ultramicroscopy, 57, 1995, pp. 45-58
37. Praprotnik, B., et al., "HV-TEM in-situ investigations of the tip shape of indium liquid metal ion emitter," Surface Science, 314, 1994, pp. 353-364
38. Driesel, W., C. Dietzsch, and R. Muhle, "In situ observation of the tip shape of AuGe liquid alloy ion sources using a high voltage transmission electron microscope," Journal of Vacuum Science & Technology B: Microelectronics and Nanometer Structures, 14, 1996, pp. 3367-3380
39. Driesel, W., et al., "In situ observation of the tip shape of Co-Ge liquid alloy ion sources in a high-voltage transmission electron microscope," Journal of Vacuum Science & Technology B: Microelectronics and Nanometer Structures, 14, 1996, pp. 1621-1629
40. Takahashi, N., "Molecular Dynamics Modeling of Ionic Liquids in Electrospray Propulsion," Aeronautics and Astronautics, Massachusetts Institute of Technology, 2010
41. Weingärtner, H., "Understanding Ionic Liquids at the Molecular Level: Facts, Problems, and Controversies," Angewandte Chemie International Edition, 47, 2008, pp. 654-670
42. *NISPLab Facilities and Equipment*. [Webpage] 2006 [2013 June 29]; Available from: http://www.nanocenter.umd.edu/labs/NISP/facilities.php.
43. *JEM-2100 Electron Microscope*. 2004 [2013 July 3]; Available from: http://www.graduate-studies-in-cancer-research.org/CIF/docs/TEM%20manual_JEOL-2100.pdf.
44. Wakai, C., et al., "How Polar Are Ionic Liquids? Determination of the Static Dielectric Constant of an Imidazolium-based Ionic Liquid by Microwave Dielectric Spectroscopy," The Journal of Physical Chemistry B, 109, 2005, pp. 17028-17030
45. Coleman, S., et al., "Investigating Nanostructuring within Imidazolium Ionic Liquids: A Thermodynamic Study Using Photochromic Molecular Probes," The Journal of Physical Chemistry B, 113, 2009, pp. 15589-15596